NASA/TM–20230015301

A Tool for Defining Tow-Steered Laminates for Finite Element Grids

Brian H. Mason, Alana M. Cardona, Erin K. Anderson, and Dawn C. Jegley
Langley Research Center, Hampton, Virginia

November 2023

NASA STI Program Report Series

Since its founding, NASA has been dedicated to the advancement of aeronautics and space science. The NASA scientific and technical information (STI) program plays a key part in helping NASA maintain this important role.

The NASA STI program operates under the auspices of the Agency Chief Information Officer. It collects, organizes, provides for archiving, and disseminates NASA's STI. The NASA STI program provides access to the NTRS Registered and its public interface, the NASA Technical Reports Server, thus providing one of the largest collections of aeronautical and space science STI in the world. Results are published in both non-NASA channels and by NASA in the NASA STI Report Series, which includes the following report types:

- TECHNICAL PUBLICATION. Reports of completed research or a major significant phase of research that present the results of NASA Programs and include extensive data or theoretical analysis. Includes compilations of significant scientific and technical data and information deemed to be of continuing reference value. NASA counterpart of peer-reviewed formal professional papers but has less stringent limitations on manuscript length and extent of graphic presentations.

- TECHNICAL MEMORANDUM. Scientific and technical findings that are preliminary or of specialized interest, e.g., quick release reports, working papers, and bibliographies that contain minimal annotation. Does not contain extensive analysis.

- CONTRACTOR REPORT. Scientific and technical findings by NASA-sponsored contractors and grantees.

- CONFERENCE PUBLICATION. Collected papers from scientific and technical conferences, symposia, seminars, or other meetings sponsored or co-sponsored by NASA.

- SPECIAL PUBLICATION. Scientific, technical, or historical information from NASA programs, projects, and missions, often concerned with subjects having substantial public interest.

- TECHNICAL TRANSLATION. English-language translations of foreign scientific and technical material pertinent to NASA's mission.

Specialized services also include organizing and publishing research results, distributing specialized research announcements and feeds, providing information desk and personal search support, and enabling data exchange services.

For more information about the NASA STI program, see the following:

- Access the NASA STI program home page at http://www.sti.nasa.gov

- Help desk contact information:

https://www.sti.nasa.gov/sti-contact-form/
and select the "General" help request type.

NASA/ TM–20230015301

A Tool for Defining Tow-Steered Laminates for Finite Element Grids

Brian H. Mason, Alana M. Cardona, Erin K. Anderson, and Dawn C. Jegley
Langley Research Center, Hampton, Virginia

National Aeronautics and
Space Administration

Langley Research Center
Hampton, Virginia 23681-2199

November 2023

Available from:

NASA STI Program / Mail Stop 148
NASA Langley Research Center
Hampton, VA 23681-2199
Fax: 757-864-6500

Nomenclature

b	Distance from arc center to the chord of an arc
c	Boolean variable used to indicate concavity of an arc, 1=concave, -1=convex
d	Distance between arc endpoints, global x-direction
e	Distance between arc endpoints, global-y direction
f	Total length of panel, global x-direction
g	Total width of panel, global y-direction
h	Half-wavelength of a course of circular arcs
j	Course-shift distance, x′-direction
k	Course-shift distance, y′-direction
m	Index for courses in a ply
n	Index for arcs in a course
p	Distance between center of an arc and another point in the panel
p_i	Shortest distance between the arc center and the inner edge of the course
p_o	Shortest distance between the arc center and the outer edge of the course
$q_i^{m,n}$	Distance between arbitrary point *i* in a panel and the center of arc *n* of course *m*
r	Radius of curvature of a course centerline
s	Shift distance between courses in a ply
s_g	Shift distance for maximum gap between courses that touch at one point
s_o	Shift distance for maximum overlap between courses that touch at one point
t	Thickness of a ply
u	Length of enclosure zone for coverage of a panel, x′-direction
v	Width of enclosure zone for coverage of a panel, y′-direction
w	Width of a single course
x	Ordinate axis of global coordinate system
x_0	Origin of initial arc, global x-direction
x'	Ordinate axis of local coordinate system rotated by ϕ from the global system
y	Abscissa axis of global coordinate system
y_0	Origin of initial arc, global y-direction
y'	Abscissa axis of local coordinate system rotated by ϕ from the global system
z	Width of boundary zone of panel
M	Number of courses in a ply
N	Number of arcs in a course
X	Center of the initial arc in initial course, global x-direction
$X^{m,n}$	Center of the arc *n* in course *m*, global x-direction
Y	Center of the initial arc in initial course, global y-direction
$Y^{m,n}$	Center of the arc *n* in course *m*, global y-direction
α	Angle of starting point of initial arc relative to the arc center
α^n	Angle at starting point of arc *n* relative to the arc center
$\delta\alpha$	Sweep angle of initial arc
$\delta\alpha^n$	Sweep angle of arc *n*
β	Gap variable, expressed as percentage of shift distance between s_o and s_g
ϕ	Course angle
θ_0	Tangent angle at starting point of arc segment
θ_1	Tangent angle at ending point of arc segment
ψ	Shift angle between courses in a ply

Executive Summary

Tailoring of composite laminates is traditionally performed by changing the orientation of straight fibers in one or more plies. Modern automated fiber placement machines facilitate placement of bundles of curved fibers (tows) in a process called tow-steering, but additional variables must be used to define the shapes of tow-steered fiber paths. In this paper, a Python-based tool, called Automated Tool for Steered COmposite Optimizable Laminates (ATSCOOL), is presented for modeling steered tows as chains of circular arcs. The geometry for defining tow path shapes using four input variables is described. The formulae for determining gaps and overlaps between clusters of consecutive tows, called courses, and for determining the number of steered courses needed to cover a rectangular panel are presented. Graphical representation of courses and thickness distribution in an example panel using the ATSCOOL software are presented. Finally, an example of a finite element analysis performed using the property information output from ATSCOOL is shown.

I. Introduction

The NASA Advanced Air Transport Technology (AATT) project is tasked with researching technologies to drastically reduce fuel consumption, noise, and emissions in the next generation of aircraft, with a focus on subsonic fixed-wing commercial transports. Within AATT, the use of a structurally efficient transonic truss-braced wing (TTBW) is under consideration to accomplish these goals. One TTBW concept under consideration is the subsonic ultra-green aircraft research (SUGAR) concept, which is designed to operate efficiently at a cruise speed of Mach 0.80 [1].

The SUGAR design is predicted to reduce fuel consumption by 7% to 9% compared to traditional tube and cantilever wing single-aisle transport aircraft [1]. Critical to the fuel-efficiency requirement of SUGAR and other TTBW designs is a process to create a low-weight structural design. In the concept shown in Fig. 1, a low-weight but high-stiffness wing design is especially important due to its large aspect ratio of 19.56. To counteract the weight increase of the added struts to support the thin wing, mass savings from other components such as the wing cover panels, ribs, and spars are needed. The manufacturing process for the TTBW design must also be cost- and time-efficient. A manufacturing method commonly used today for composite transport wings is automated fiber placement (AFP). One manufacturing system capable of performing AFP is the Integrated Structural Assembly of Advanced Composites (ISAAC) [2] robotic system at NASA Langley Research Center, as illustrated in Fig. 2.

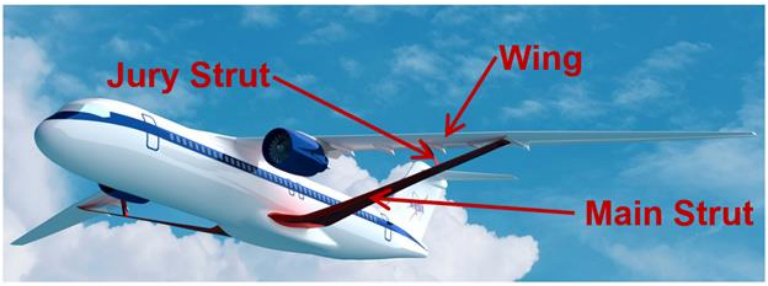

Fig. 1. TTBW concept.

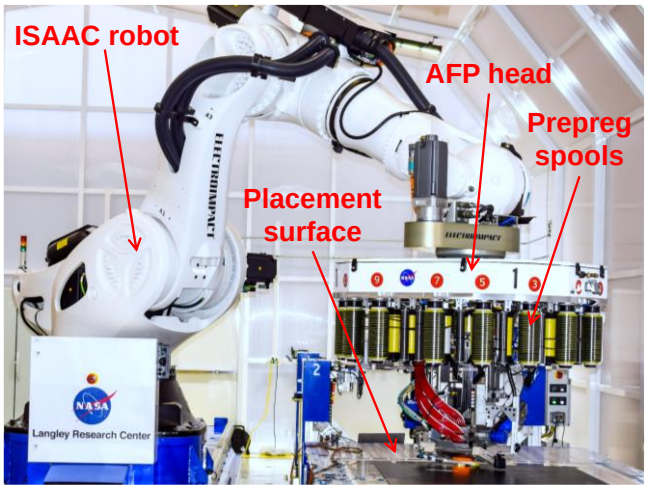

Fig. 2. ISAAC manufacturing robotic system.

In AFP, fibers are traditionally placed in straight paths in every ply of the laminate, resulting in laminates that resemble those fabricated via manually-placed material. However, AFP facilitates fibers to change direction within a ply by programming curvilinear paths into the robotic controls, which enables a more tailored design. Whether straight or curvilinear fiber paths are used, numerous fiber bundles, called "tows," are typically fed from a spool and placed on a tool during AFP. Several tows, all with the same width, placed simultaneously in a preprogrammed path are identified as a "course" of tows. For example, ISAAC can be used to place up to sixteen ¼-inch-wide tows in one

course. Typically, a ply consists of multiple courses. Changing fiber orientation within a ply is called "tow steering." Tow-steered composite designs offer the opportunity for greater stiffness and strength tailoring when compared with standard straight-fiber designs.

Tow-steering facilitates the manufacture of laminates with curvilinear fiber paths that can provide more structurally efficient load path tailoring than straight fiber designs [3 - 7]. However, analytical tools are needed to design and analyze tow-steered components. One complication in analytical simulation of tow-steered structures is the creation of gaps and overlaps between tows in a laminate, which results in laminates with a non-constant thickness. An overlap occurs during AFP when a tow or partial tow lies atop another tow in the same ply, resulting in a local thickening of the laminate. Similarly, a gap is a void between tows within a single ply. Analytical approaches that account for local changes in the angles of the steered fibers but treat the laminates as constant thickness by ignoring gaps and overlaps are described in Ref. [8]. Such approaches ignore the potential stiffening benefits of the overlaps which act as integral stiffeners. Some studies have been undertaken to account for these thickness changes [5 - 7], but these algorithms require tedious iteration along each course path to determine locations of gaps and overlaps. Use of circular arcs to define some of the geometry for tow placement (e.g., calculation of the distance between tow-steered courses and calculation of the number of tow-steered courses needed to cover a panel), was mentioned in reference [7], but formulation of this approach was not presented and has not been found in a recent literature search. In this paper, the circular arc formulation for computing tow-steered geometry is derived.

The goal of this paper is to present a new analytical tool to define laminate properties in a finite element model (FEM) that simulates gaps, overlaps, and local angle changes in tow-steered composites. This Python-based software is called Automated Tool for Steered COmposite Optimizable Laminates (ATSCOOL). First, the algorithms to perform tow-steering with a series of circular arcs are described. Next, details for running the ATSCOOL software are provided along with a description of the required input files. Example images produced using the software for visualization of the tow-steered designs are also shown. Finally, a numerical example of a structural analysis based on the property data generated with ATSCOOL is presented.

II. Algorithms for Tow-Steering

The ATSCOOL software generates tow-steered designs of flat laminates. Each course is represented by a chain of circular arcs. The overlap of the courses can be seen in Fig. 3 where some courses appear narrower than others because parts of the courses overlap so the one underneath is hidden. The ends of the courses form a saw-tooth shape which is undesirable in the finished panel; so, the panel (with dimensions *f* by *g*) is manufactured with a boundary zone (of width z) as shown in Fig. 3. Also, in AFP the ends of the tows in a course tend to wander at the start and end of a course (due to issues such as not sticking well to the placement surface), so the boundary zone is used to represent the typical distance with wandering. The length of each course is determined by the dimensions of the full panel. A series of courses are placed, and each course is shifted by a specified distance in a specified direction from the neighboring courses. The variables and formulae used to define the courses are presented in the following paragraphs.

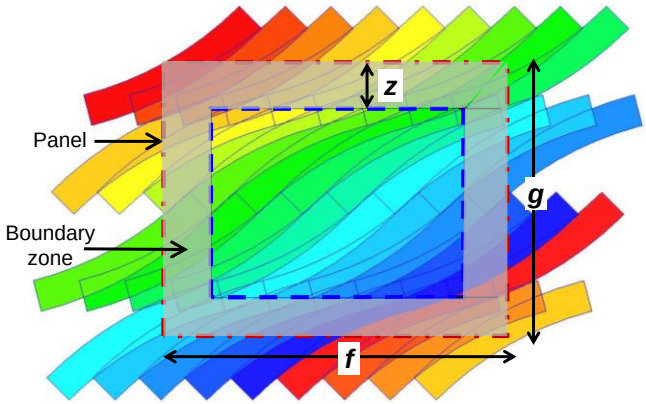

Fig. 3. Course paths of repeated circular arcs.

A. Definition of Initial Arc in a Course

In the ASCOOL software, three independent input variables are used to define the center of the initial curve in each ply: course angle (ϕ), radius of curvature (r), and chord length between the ends of the arc (h). A fourth variable (c) to determine if the arc is concave (c is +1) or convex (c is -1). For the purposes of the formulae in this paper, the initial curve is considered to be concave if the cross product of vectors b and h is positive. The center of curvature (X, Y) of the initial arc is computed from these variables. The first step in determining the arc center is to define a line b that bisects the arc and is normal to the line h between the endpoints of the arc, as shown in Fig. 4, using Equations (1) through (3).

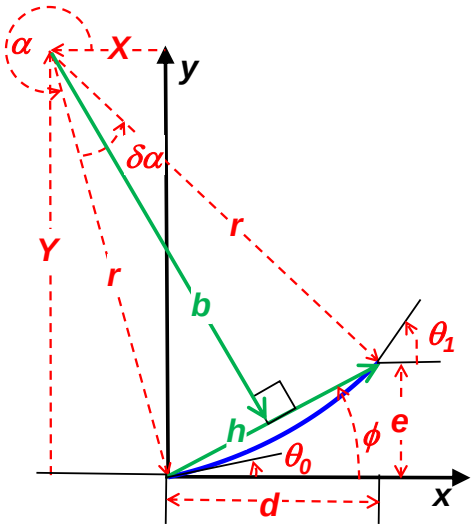

Fig. 4. Definition of initial arc (for concave arc, $c > 0$).

$$b = \sqrt{r^2 - 0.25\,h^2} \quad (1)$$
$$d = h\,\cos(\phi) \quad (2)$$
$$e = h\sin(\phi) \quad (3)$$

The arc center is defined with Equations (4) and (5), where the variable c has a value of 1 for a concave curve and -1 for a convex curve.

$$X = \tfrac{1}{2}d - b\,c\sin(\phi) \quad (4)$$
$$Y = \tfrac{1}{2}e + b\,c\cos(\phi) \quad (5)$$

The initial arc angle (α) and sweep angle ($\delta\alpha$) are computed from the following equations

$$\alpha = \tan^{-1}\left(\frac{-Y}{-X}\right) \quad (6)$$
$$\delta\alpha = \tan^{-1}\left(\frac{e-Y}{d-X}\right) - \alpha. \quad (7)$$

The sweep angle is positive if the arc is concave (sweeping in clockwise direction about the origin) and negative if the arc angle is positive (sweeping in the counterclockwise direction). Two variables, θ_0 and θ_1, define the tangent angle at either end of the arc. The values of θ_0 and θ_1 are computed from Equations (8) and (9).

$$\theta_0 = \alpha + 90° \quad (8)$$
$$\theta_1 = \alpha + \delta\alpha + 90° \quad (9)$$

B. Definition of a Chain of Arcs in a Course

Next, it is necessary to define the other arcs in the chain. Two indices, m and n, are used to identify the course number and the arc in the chain for that course, respectively. These indices are used as superscripts for the arc centers ($X^{m,n}$ and $Y^{m,n}$), as shown in Fig. 5. The base course is identified by an index value (m) of zero and the base curve in each course is identified with another index value (n) of zero. As illustrated in Fig. 5, the centers of the arcs ($X^{m,n}$, $Y^{m,n}$) are mirrored about the line defined by the course angle (ϕ). Curves with an even curve index number are defined with the Equations (10) to (13).

$$\alpha^{even} = \alpha \quad (10)$$
$$\delta\alpha^{even} = \delta\alpha \quad (11)$$
$$X^{0,even} = X + n\,d \quad (12)$$
$$Y^{0,even} = Y + n\,e \quad (13)$$

Curves with an odd curve index number are defined with the Equations (14) to (17).

$$\alpha^{odd} = \alpha + 180° \quad (14)$$
$$\delta\alpha^{odd} = -\delta\alpha \quad (15)$$
$$X^{0,odd} = -X + (n+1)\,d \quad (16)$$
$$Y^{0,odd} = -Y + (n+1)\,e \quad (17)$$

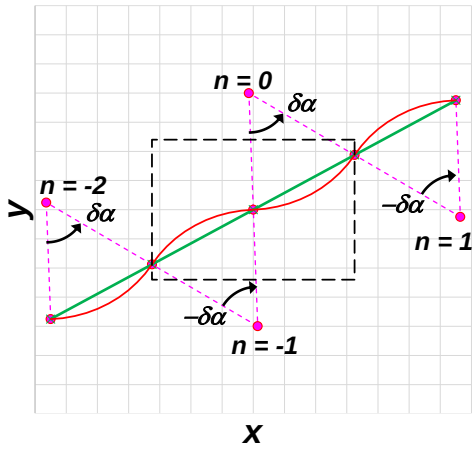

Fig. 5. Definition of chain of arcs to represent a course.

C. Calculation of Gap and Overlap

After the geometry of the circular arcs defining the shape of a single course is defined, the pattern for placing enough courses to define an entire layer is necessary. Three terms are needed to define the pattern for the remaining courses: a course width (w), a shift direction (ψ), and a shift distance (s). The shift distance variable is defined in terms of a maximum gap distance (s_g) and a maximum overlap distance (s_o). The maximum gap distance is the distance at which the curved boundaries of two courses intersect at one point and the courses do not overlap, as shown in Fig. 6a. The maximum overlap distance is the distance at which the curved boundaries of two courses intersect at one point and the courses overlap at every other point along the curve, as shown in Fig. 6b.

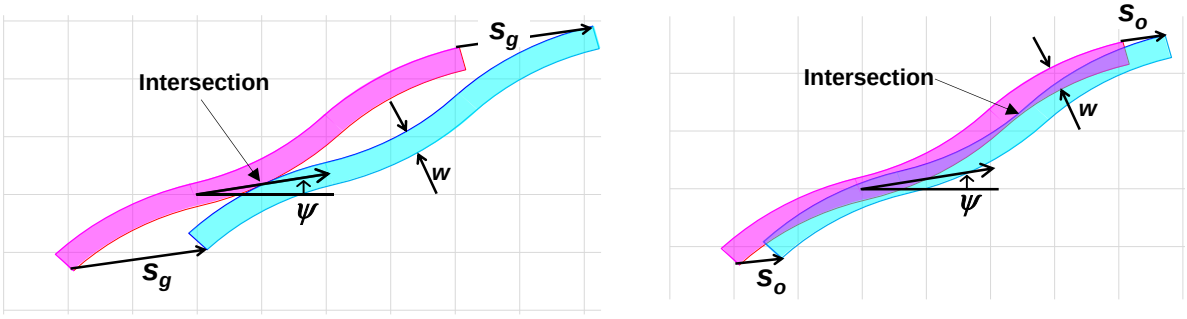

a) Maximum gap **b) Maximum overlap**

Fig. 6. Overlaps and gaps between two courses.

In both cases, the curve intersections occur at locations that are tangent to both boundary curves. Within the ATSCOOL software, a gap variable (β) is defined to have a value of zero at maximum overlap and a value of one at maximum gap, as given in Equation (18). The values of the maximum overlap and gap are derived by comparing the location of three arcs of the initial course with three arcs from a new shifted course in a process described below.

$$s = s_o + \beta\left(s_g - s_o\right) \tag{18}$$

Consider three arcs of a course (with course index number m=0) from index values (n) of -1, 0, and 1, as shown in Fig. 7. A new course (with course index number m=1) is desired at a shift distance (s) in the shift direction (ψ) from course m=0. In the example in Fig. 7, course 0 (at arc {0, 0}) and course 1 (at arc {1, -1}) touch at a single point corresponding to a maximum gap shift, as shown in Fig. 6a. The intersection point occurs at the outer edges (relative to the arc centers) of each course. If a line is used to connect the center of arc {0, 0} with arc {1, -1}, then the two

curves intersect at one point at a distance p_o from the arc centers (line BD) as given in Equation (19). In the example in Fig. 8, course 0 (at arc {0, 1}) and course 1 (at arc {1, 0}) touch at a single point corresponding to a maximum overlap shift, as shown in Fig. 6b. The intersection point occurs at the inner edges (relative to the arc centers) of each course. If a line is used to connect the center of arc {0, 1} with arc {1, 0}, then the two curves intersect at one point at a distance p_i from the arc centers (line EC) as given in Equation (20).

$$p_o = 2\,r + w \tag{19}$$

$$p_i = 2\,r - w \tag{20}$$

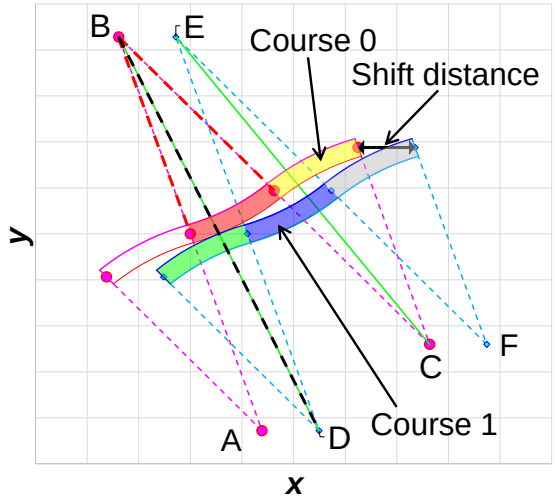

Center	{Course, Arc} {m, n}	Color
A	{0, -1}	
B	{0, 0}	
C	{0, 1}	
D	{1, -1}	
E	{1, 0}	
F	{1, 1}	

Fig. 7. Calculation of maximum gap between two courses.

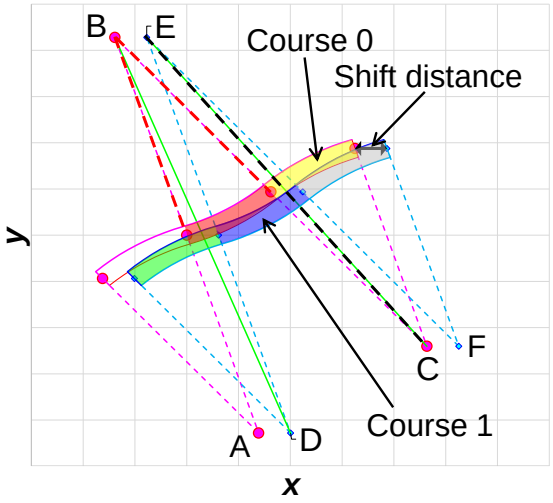

Center	{Course, Arc} {m, n}	Color
A	{0, -1}	
B	{0, 0}	
C	{0, 1}	
D	{1, -1}	
E	{1, 0}	
F	{1, 1}	

Fig. 8. Calculation of maximum overlap between two courses.

To determine the maximum gap (s_g) and maximum overlap (s_o) distances between two courses with identical shapes, it is necessary to compare the intersection points between combinations of arcs between the two courses. Based upon a study of the geometry of a few representative course shapes, checking two combinations of arc centers in the ATSCOOL software is assumed to be sufficient to determine s_g and s_o. The course and arc combinations selected are a) {0, 0} and {1, -1} and b) {1, 0} and {0, 1}, as shown in Figs. 7 and 8 with black dashed lines. The method for computing the arc center distances as a function of the shift distance is presented below.

Six arc centers in Fig. 7 are labeled A, B, C, D, E, and F, and are centers for courses and arcs {0, -1}, {0, 0}, {0, 1}, {1, -1}, {1, 0}, and {1. 1}, respectively. The coordinates for points A, B, and C for course 0 are determined using Equations (12), (13), (16), and (17) and are given in Equations (21-26).

$$X^{\mathrm{A}} = X^{0,-1} = -X \tag{21}$$
$$Y^{\mathrm{A}} = Y^{0,-1} = -Y \tag{22}$$
$$X^{\mathrm{B}} = X^{0,0} = X \tag{23}$$
$$Y^{\mathrm{B}} = Y^{0,0} = Y \tag{24}$$
$$X^{\mathrm{C}} = X^{0,1} = -X + 2d \tag{25}$$
$$Y^{\mathrm{C}} = Y^{0,1} = -Y + 2e \tag{26}$$

The coordinates for the three points for course 1 (D, E, and F) are computed by adding the shift vector to the arc centers from course 0 as given in Equations (27-32).

$$X^{\mathrm{D}} = X^{1,-1} = -X + s\cos(\psi) \tag{27}$$
$$Y^{\mathrm{D}} = Y^{1,-1} = -Y + s\sin(\psi) \tag{28}$$
$$X^{\mathrm{E}} = X^{1,0} = X + s\cos(\psi) \tag{29}$$
$$Y^{\mathrm{E}} = Y^{1,0} = Y + s\sin(\psi) \tag{30}$$
$$X^{\mathrm{F}} = X^{1,1} = -X + 2d + s\cos(\psi) \tag{31}$$
$$Y^{\mathrm{F}} = Y^{1,1} = -Y + 2e + s\sin(\psi) \tag{32}$$

Next, the distance between the two pairs of arc centers listed above (line BD from Fig. 7 and line EC from Fig. 8) must be computed using Equations (33) and (34).

$$p_{\mathrm{BD}} = \sqrt{(X^{\mathrm{B}} - X^{\mathrm{D}})^2 + (Y^{\mathrm{B}} - Y^{\mathrm{D}})^2} \tag{33}$$
$$p_{\mathrm{EC}} = \sqrt{(X^{\mathrm{E}} - X^{\mathrm{C}})^2 + (Y^{\mathrm{E}} - Y^{\mathrm{C}})^2} \tag{34}$$

The desired shift distance (s) can be computed as a function of the distance between the connecting arc centers. The shift distance must be computed twice. The shift distance (s) is computed by substitution of Equations (23-30) into Equations (33) and (34) and rearranging to create Equations (35) and (36). In Equations (35) and (36), the two different shift distances (s) are assigned subscripts corresponding to the two arc center points shown in Fig. 7. In Equations (35) and (36), the value of the variable p is defined by either Equation (19) or Equation (20), depending on whether the maximum gap distance or maximum overlap distance, respectively, is desired.

$$s_{\mathrm{BD}}^2 - 4(X\cos(\psi) + Y\sin(\psi))\, s_{\mathrm{BD}} + (4X^2 + 4Y^2 - p^2) = 0 \tag{35}$$
$$s_{\mathrm{EC}}^2 - 4\big((X-d)\cos(\psi) + (Y-e)\sin(\psi)\big)\, s_{\mathrm{EC}} + (4(X-d)^2 + 4(Y-e)^2 - p^2) = 0 \tag{36}$$

The solution is found using the quadratic equation.

$$s_{\mathrm{BD}} = 2(X\cos(\psi) + Y\sin(\psi)) \pm \sqrt{4(X\cos(\psi) + Y\sin(\psi))^2 - (4X^2 + 4Y^2 - p^2)} \tag{37}$$
$$s_{\mathrm{EC}} = 2\big((X-d)\cos(\psi) + (Y-e)\sin(\psi)\big) \pm \sqrt{4\big((X-d)\cos(\psi) + (Y-e)\sin(\psi)\big)^2 - (4(X-d)^2 + 4(Y-e)^2 - p^2)} = 0 \tag{38}$$

Two solutions for each distance are computed from each Equation (37) and (38), resulting in four possible values for the maximum gap distance (by substituting p_o for p) and four possible values for the maximum overlap distance (by substituting p_i for p). For each case (maximum gap or maximum overlap), the shift distance used is the lowest positive value greater than zero.

D. Course Coverage for the Entire Panel

After the course centers of curvature and shift distances have been computed, both the number of courses (M) and number of arcs per course (N) necessary to cover the entire panel must be determined. Although using a very large number of courses and arcs in the ATSCOOL software would be simpler, that approach is not computationally

efficient. To estimate the number of courses and arcs, for simplicity, the arcs are considered as rectangles. To ensure coverage of the panel, a rotated enclosure zone is defined as shown in Fig. 9. The panel is defined as a rectangle of length f and width g. For a given course angle (ϕ) the dimensions of the enclosure zone (u and v) are given by Equations (39) and (40).

$$\mathrm{u} = f|\cos\phi| + g|\sin\phi| \tag{39}$$
$$\mathrm{v} = f|\sin\phi| + g|\cos\phi| \tag{40}$$

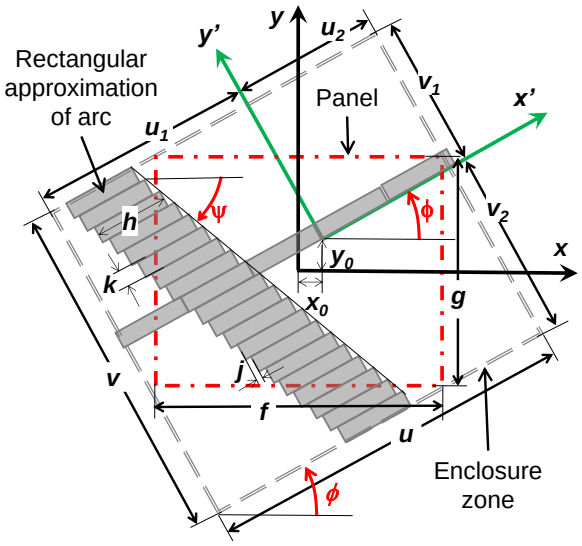

Fig. 9. Enclosure zone used to estimate number of courses and arcs to cover a panel.

The origin of the initial arc of course 0 is located at a defined starting point (x_0, y_0), but to evaluate panel coverage, this origin point must transform into the rotated coordinate system (x', y') using Equations (43) and (44). The enclosure zone is divided into four sections divided by the axes of the rotated coordinate system as shown in Fig. 9. The dimensions of each section are given by dimensions u_1, u_2, v_1, and v_2, as computed using Equations (45-48). The number of courses and arcs can be estimated by approximating each arc as a rectangle of length (h) and width (k), per Equation (50). The course index (m) varies from $-M_1$ to M_2, and the arc index (n) varies from $-N_1$ to N_2, as given in Equations (51-54), in which the ceiling function (ceil) represents rounding up to the next integer.

$$x' = x_0\cos\phi + y_0\sin\phi \tag{43}$$
$$y' = -x_0\sin\phi + y_0\cos\phi \tag{44}$$
$$u_1 = \frac{u}{2} + x_0\cos\phi + y_0\sin\phi \tag{45}$$
$$u_2 = u - u_1 \tag{46}$$
$$v_1 = \frac{v}{2} - x_0\sin\phi + y_0\cos\phi \tag{47}$$
$$v_2 = v - v_1 \tag{48}$$
$$j = s\,|\cos(\phi - \psi)| \tag{49}$$
$$k = s\,|\sin(\phi - \psi)| \tag{50}$$
$$N_1 = \mathrm{ceil}\left(\frac{v_1}{k}\right) \tag{51}$$
$$N_2 = \mathrm{ceil}\left(\frac{v_2}{k}\right) \tag{52}$$
$$M_1 = \mathrm{ceil}\left(\frac{u_1 + j\max(N_1,N_2)}{h}\right) \tag{53}$$
$$M_2 = \mathrm{ceil}\left(\frac{u_2 + j\max(N_1,N_2)}{h}\right) \tag{54}$$

E. Mapping Tow-Steered Courses onto a FEM Grid

To facilitate structural analysis, a methodology is needed to map fiber orientations within each tow-steered layer onto a pre-defined FEM grid. To begin the mapping process, point *i* representing the center of an element located at (x_i, y_i) is selected, as shown in Fig. 10. Next, a vector is defined between the selected point and the center of a selected circular arc *n* of a selected course *m*. The angle (α_i) and length ($q_i^{m,n}$) of this vector are computed using Equations (55) and (56), respectively. The selected point lies within the arc segment if it is between the inner and outer radii of the arc and is within the sweep angle of the arc. The selected point is determined to lie on arc *n* of course *m* if $q_i^{m,n}$ satisfies the conditions in Equation (57) and α_i is between $\alpha^{m,n}$ and $\alpha^{m,n} + \delta\alpha^{m,n}$. This process is repeated for all arcs in all courses in the tow-steered layer. Note that a given point can lie on more than one course or on no courses, in the case of an overlap or gap, respectively. For example, in Fig. 10, point *i* lies within courses {0,0} and {1,0}, but not within course {1,-1} because the line from D to *i* is not within the arc of that course.

The ATSCOOL software is used to create an array of ply angles, ply materials, and ply thicknesses by looping over all element centroids and evaluating these centroids against all arcs in all courses in every ply. A section property card is written for every element as a laminated composite shell element that contains the full stack up (including overlaps) at each element centroid. In the section property card, overlaps are represented as additional plies, while gaps are represented as missing plies. A finite element input file with a unique property defined for each element may require a significant amount of pre-processing computational effort due to the size of the input file. In a future version of the ATSCOOL software, methods for reducing the input file size by evaluating fiber-angle fidelity will be implemented.

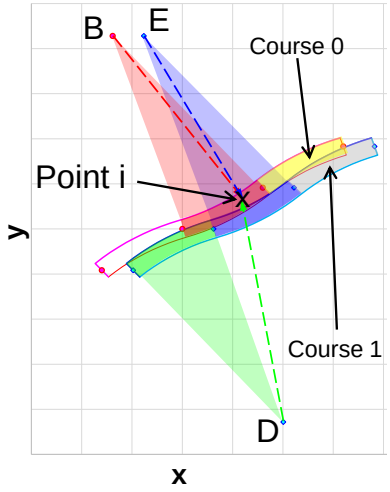

Center	{course, arc} {m, n}	Color
A	{0, -1}	
B	{0, 0}	
C	{0, 1}	
D	{1, -1}	
E	{1, 0}	
F	{1, 1}	

Fig. 10. Mapping fiber orientation onto FEM grid.

$$\alpha_i = \tan^{-1}\left(\frac{Y_i - Y^{m,n}}{X_i - X^{m,n}}\right) \tag{55}$$

$$q_i^{m,n} = \sqrt{(X_i - X^{m,n})^2 + (Y_i - Y^{m,n})^2} \tag{56}$$

$$h - \frac{w}{2} \le q_i^{m,n} \le h + \frac{w}{2} \tag{57}$$

F. Summary of Circular-Arc Tow-Steering Algorithms and Additional Parameters

In the ATSCOOL software, four variables are used to define the shape of the primary arc in the initial course: course angle (ϕ), radius of curvature (r), length between the ends of the arc (h), and a concavity Boolean (c). Three terms are needed to define the pattern for the other courses: a course width (w), a shift direction (ψ), and a gap percentage (β). Although the primary arc described in this section was assumed to start at the origin of the coordinate system (x=0, y=0), two variables (x_0 and y_0) are available in ATSCOOL to shift the coordinates of all tows in the software by a defined distance from the center.

III. ATSCOOL Graphical User Interface

The graphical user interface (GUI) for ATSCOOL is shown in Fig. 11. The GUI is operated from the top down and follows the order of execution described below:

1. Read laminate data
2. Inspect tow-steered layers
3. Write tow paths for AFP
4. Select FEM grid file
5. Name the output files
6. Map tow data to the FEM grid
7. Inspect thicknesses mapped onto the finite element grid

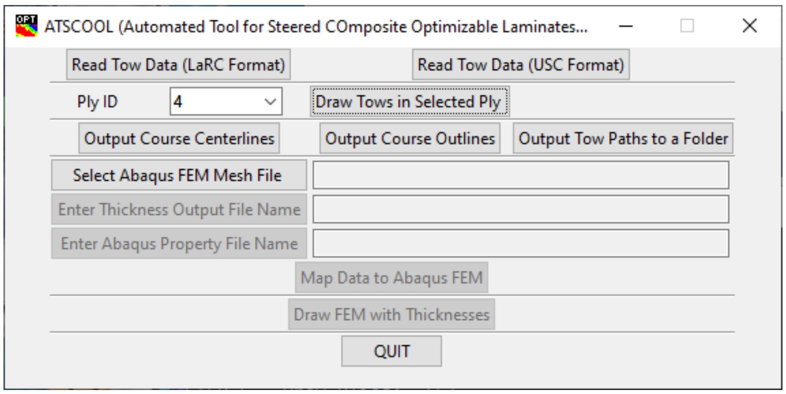

Fig. 11. GUI for ATSCOOL.

A. Laminate Input File Format

The two buttons at the top of the ATSCOOL GUI are used to import a text file defining the layup sequence of the panel. A sample input file is shown in Fig. 12. In the input file, the variables defined in this paper are identified with short labels. The first line of the input file contains the panel information including panel length (xdim), panel width (ydim), boundary zone width (lead), total number of layers (nplies), and the symmetry status for the panel. Each layer is defined with straight-fiber courses or courses that are chains of circular arcs. For straight fibers, only three variables are provided: material number (matlID), ply thickness (t), and course angle (phi). For a curvilinear fiber, ten variables must be provided: material number (matlID), ply thickness (t), course angle (phi), half-wavelength (len), radius of curvature (radius), shift angle (shift), course width (course), gap percentage (gap), and origin of initial course (x0, and y0). Note that the sign of the len input value is used to determine the value of the concave Boolean variable (c). The ply thickness and material number are not used in defining the shape of the courses, but those variables are used to define the section property information for the FEM grid.

```
&PANEL_DATA       xdim=32.5000  ydim=23.5000  lead=4.00 /

&LAYUP_PARAMETERS  nplies=27  symmetric=true /

&PLY_DATA       matlID=1 t=0.0055 method='Constant'     phi=+45.0000 /
&PLY_DATA       matlID=1 t=0.0055 method='Constant'     phi=-45.0000 /
&PLY_DATA       matlID=1 t=0.0055 method='Constant'     phi=+45.0000 /
&PLY_DATA       matlID=1 t=0.0055 method='Constant'     phi=-45.0000 /
&PLY_DATA       matlID=1 t=0.0055 method='CircularArc'  phi=+22.5000 len=-30.7042 radius=45.00  shift=+0.00 course=4.00 gap=0.00  x0=+0.00 y0=+0.00 /
&PLY_DATA       matlID=1 t=0.0055 method='CircularArc'  phi=-22.5000 len=+30.7042 radius=45.00  shift=+0.00 course=4.00 gap=0.00  x0=+0.00 y0=+0.00 /
&PLY_DATA       matlID=1 t=0.0055 method='CircularArc'  phi=+22.5000 len=-30.7042 radius=45.00  shift=+0.00 course=4.00 gap=0.00  x0=+0.00 y0=+0.00 /
&PLY_DATA       matlID=1 t=0.0055 method='CircularArc'  phi=-22.5000 len=+30.7042 radius=45.00  shift=+0.00 course=4.00 gap=0.00  x0=+0.00 y0=+0.00 /
&PLY_DATA       matlID=1 t=0.0055 method='CircularArc'  phi=+22.5000 len=-30.7042 radius=45.00  shift=+0.00 course=4.00 gap=0.00  x0=+0.00 y0=+0.00 /
&PLY_DATA       matlID=1 t=0.0055 method='CircularArc'  phi=-22.5000 len=+30.7042 radius=45.00  shift=+0.00 course=4.00 gap=0.00  x0=+0.00 y0=+0.00 /
&PLY_DATA       matlID=1 t=0.0055 method='Constant'     phi=+90.0000 /
&PLY_DATA       matlID=1 t=0.0055 method='Constant'     phi=-90.0000 /
&PLY_DATA       matlID=1 t=0.0055 method='Constant'     phi=+0.0000 /
&PLY_DATA       matlID=1 t=0.0055 method='Constant'     phi=+90.0000 /
```

Fig. 12. Input file format.

B. Inspection of Steered Tows

In the second row of the GUI, the user can use a drop-down list to select a tow-steered ply by its number and then generate an image showing the tow centerlines for that layer. An example of a tow-steered layer is shown in Fig 13. The plot includes an outline of the panel (red dot-dashed rectangle) and the boundary zone (blue dashed rectangle). In the plot, a black arrow is used to represent the shift direction between each course. Typically, a boundary distance of 4 in. on each edge is needed due to tow wandering that can occur during the first and last 4 in. of a course, but the designer can plan for any distance.

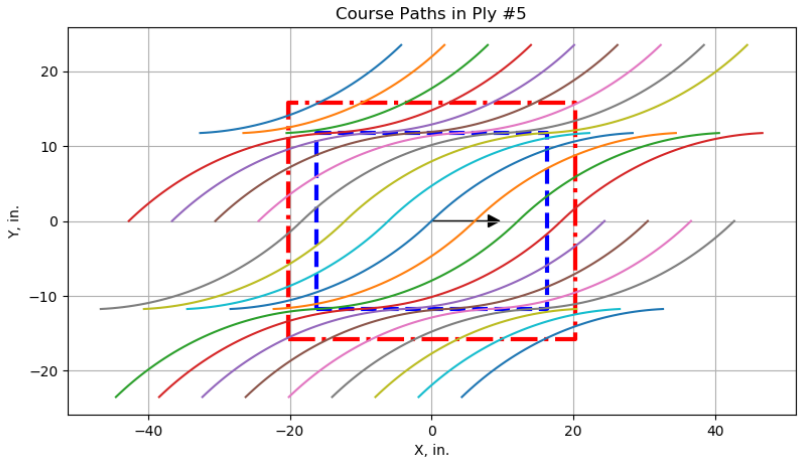

Fig. 13. Example of course centerline plot output from ATSCOOL GUI.

C. Output of Tow Paths for AFP

On the third row of the GUI, three buttons enable the user to output the geometry of the courses. The three options are: course centerlines for the currently selected ply (from line 2), outlines of the courses for the currently selected ply, and output of all course centerlines to a folder. The centerline coordinates for each course can be exported from ATSCOOL for use in AFP machines.

Output of the geometry from the currently selected ply is written to a text session file for the PATRAN finite element modeling software [9]. For the PATRAN output, the courses are written as a series of commands to create points and then create circular arcs connecting theses points. A final set of commands is used to merge the circular arcs into single curves. To use the PATRAN curves in an AFP robotic system, the user must first create a PATRAN database, run the session file, and finally export the curves to an appropriate geometry file format that can be used by the software that is used to program the AFP robot.

The output format for the third option (folder output) is comma separated value (CSV) text file. The ATSCOOL user can create a folder for the panel, and a subfolder will be generated for each tow-steered layer. For the CSV output, a single file is created for each tow-steered course in a layer. The values written to the CSV file are an array of x-coordinates, y-coordinates, and local angles to define a tow course. Note the geometry data is transformed into the coordinate system of the AFP robotic system.

D. Select FEM Grid File

The button on the fourth row of the GUI lets the user select a FEM grid for mapping laminate properties. ATSCOOL can be used to read in the nodes and element connectivity for a FEM grid. Currently, the software is limited to importing data consistent with the ABAQUS finite element analysis code [10]. The input file must include a single list of nodes (beginning with one *NODE card) and a list of quadrilateral shell elements. Presently, only element types S4 and S4R are supported.

E. Output Files

The controls on the fifth and sixth lines of the GUI allow the user to output ATSCOOL property data to a thickness file and/or a FEM property file. The map button on the seventh line of the GUI activates the ATSCOOL mapping function described in Section II.E. The mapping function can be used to compute the geometric center for every element and use that vector of coordinates for determining the stacking sequence for the laminate at that point. Variation of laminate properties (e.g. local changes in gaps, overlaps, and ply angles) within a given element are not considered due to the nature of the mapping approximation.

The first output file is a text file containing a list of element ID numbers with the corresponding integer number of plies for each layer. The second file is a list of laminate section property cards and ABAQUS element sets. The stacking sequence is defined using the thickness and material numbers from the input file, and the ply angles computed in Section II.E. For the ABAQUS format, the data is written as a *SHELL SECTION card. The offset is set to -0.5, because the initial ply of the laminate is defined as the bottom ply in the stacking sequence and typically represents the outer mold line (OML) in aerospace structures. While the OML is considered to be a smooth or flat surface, the inner mold line (IML) will have raised areas due to gaps and overlaps.

F. Inspection of Mapped Tow Data

The button on the ninth line of the GUI allows the user to generate a thickness plot of the full panel to visualize the effect of the gaps and overlaps, as shown in Fig. 14. Thicker areas are shown in red, and thinner areas are shown in blue. The thickness label is provided as a number of plies instead of an actual thickness in units of length.

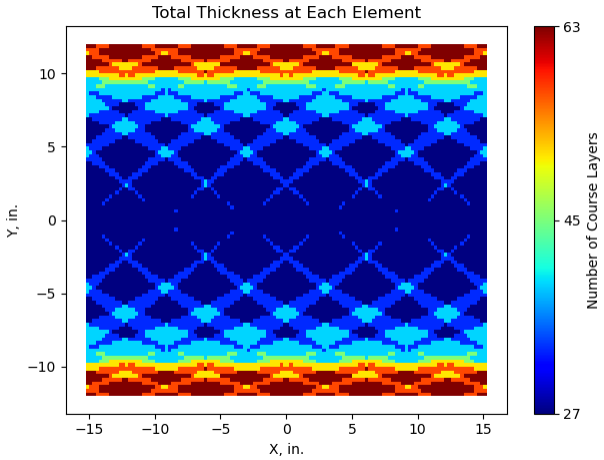

Fig. 14. Example of thickness plot output from ATSCOOL GUI.

IV. Numerical Test Case

To demonstrate how ATSCOOL can be used to define laminate properties for a tow-steered panel, an example problem is presented in this section. Finite element analysis (FEA) is the preferred technique for computational simulation of responses for structures with complicated geometry. The FEM used as a test case in this paper consisted of 11,712 shell (quadrilateral) elements and 11,931 nodes. Each element was a square with an edge length of 0.25 in. The panel dimensions were 32.5 in. in length (x-direction) and 24.0 in. in width (y-direction). The stacking sequence was defined as $[\pm 45_2/(\pm 30^{r45h24})_3/90_2/0/90]_S$, in which the superscript r45 represents a curved course with a 45 in. radius and the superscript h24 represents a tow half-wavelength of 24 in. In terms of the ATSCOOL input format, the curved tow data for plies 5 and 6 are provided in Table 1 and are illustrated in Figs. 15 and 16. Note that plies 7 and 9 are identical to ply 5, and plies 8 and 10 are identical to ply 6.

Table 1. Variables for plies 5 and 6.

Input File Term	Variable(s) (see Section II)	Description	Ply 5 Input (also 7 and 9)	Ply 6 Input (also 8 and 10)
phi	ϕ	Course angle	30.0°	30.0°
len	$h * c$	Half-wavelength * concave variable	-24.0 in.	24.0 in.
radius	r	Radius of curvature	45.0 in.	45.0 in.
shift	ψ	Shift angle	0.0°	0.0°
course	w	Course width	4.0 in.	4.0 in.
gap	g	Gap percentage	0.0	0.0
x0	x_0	x-origin	0.0 in.	0.0 in.
y0	y_0	y-origin	0.0 in.	0.0 in.

Fig. 15. Plot of course centerlines for example plies 5, 7, and 9.

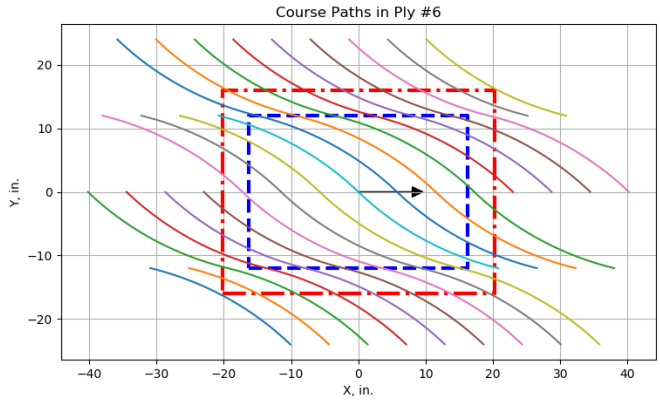

Fig. 16. Plot of course centerlines for example plies 6, 8, and 10.

The ATSCOOL software was used to map the example stacking sequence onto the FEM grid as a series of composite section property cards, one card per element. A thickness map of the laminate is shown in Fig. 17. A buckling and static FEA of the panel was performed in Abaqus. In both analyses, the edges of the panel were simply supported, and a uniform compressive edge load of 1000 lbf was applied to the vertical edges (at x=-16.25 in. and x=-16.25 in.). Material properties used are presented in Table 2. The maximum layer-wise Tsai-Hill first-ply failure indices for the panel are shown in Fig. 18, and the first four buckling mode shapes for this design are shown in Fig. 19.

Table 2. Material properties.

Property	IM7/8552 [11]
Ply Thickness, in.	0.0055
Weight Density, lbf/in.^{3}	0.05714
Elastic Modulus – Longitudinal, Msi	22.99
Elastic Modulus – Transverse, Msi	1.30
Shear Modulus, Msi	0.68
Poisson's Ratio	0.316
Tensile Strength – Longitudinal, ksi	362.69
Tensile Strength – Transverse, ksi	9.29
Compressive Strength – Longitudinal, ksi	-248.94
Compressive Strength – Transverse, ksi	-41.44
Shear Strength, ksi	13.22

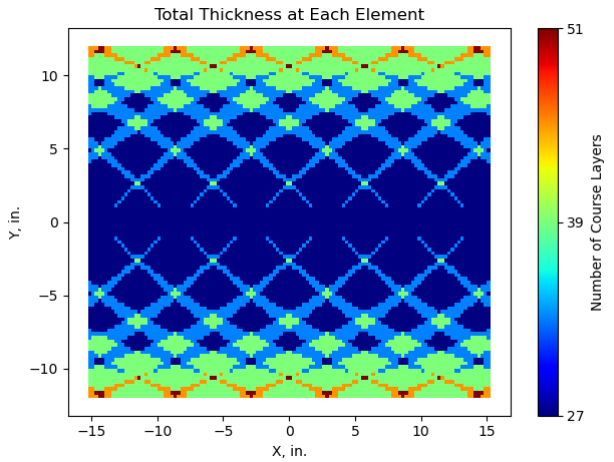

Fig. 17. Thickness plot for example laminate.

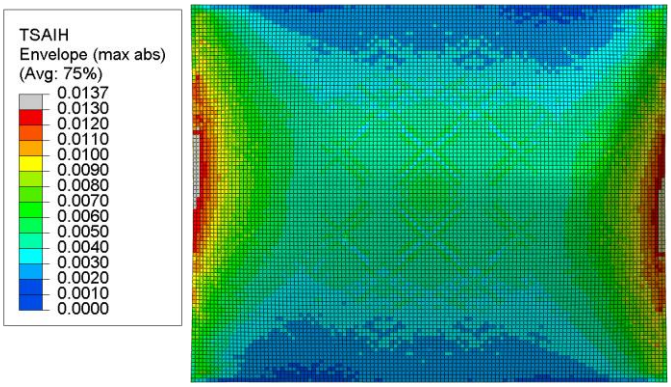

Fig. 18. Tsai-Hill failure index plot for example laminate.

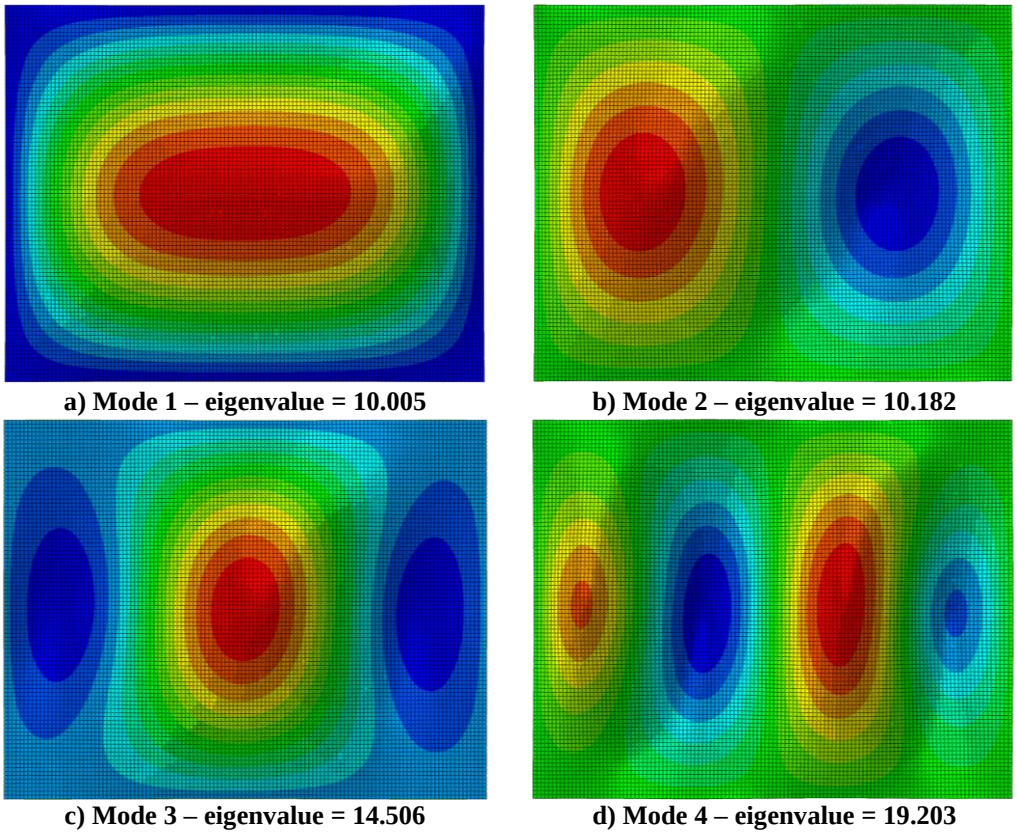

a) Mode 1 – eigenvalue = 10.005 **b) Mode 2 – eigenvalue = 10.182**

c) Mode 3 – eigenvalue = 14.506 **d) Mode 4 – eigenvalue = 19.203**

Fig. 19. First four buckling eigenmodes for example laminate.

V. Concluding Remarks

In this document, Python-based software for modeling tow-steered laminates called ATSCOOL was presented. The tool can be used to define courses of a composite laminate as chains of circular arcs and simulate those laminates in both finite element software and in a geometry file usable by automated fiber placement software tools. The theory behind the definition of chains of circular arcs using eight shape variables was presented. Variables for course angle, arc wavelength, and radius of curvature are used to define the shape of the initial arc. Variables for the shift angle, course width, and gap percentage are used to determine the distance between courses for placement. The final two x- and y-origin variables are used in conjunction with the panel dimensions to develop an algorithm to approximate the number of arcs and courses needed to cover the panel.

To demonstrate operation of the ATSCOOL tool, an example laminate was studied. Algorithms used to generate images of the tow centerlines and laminate thickness plots were shown. The user can use the ATSCOOL plotting functions to visualize placement of the courses and course shapes before any exhaustive simulation is performed. The code can also be used to program course paths for robotic placement systems. Within the tool, the numerical model transfers directly to the manufacturing program so the laminate stacking sequence of the manufactured specimens matches the design. Finally, a finite element simulation of the example tow-steered laminate was performed. The analysis using an ATSCOOL-generated laminate property deck was successfully used to simulate buckling eigenmodes and to evaluate a strength-based Tsai-Hill first-ply failure scenario for the example laminate. Future development of the ATSCOOL software is expected to include exploration of the design space using the course geometry variables defined in this paper, and evaluation of algorithms to reduce the number of property sections in the simulation models by binning individual elements into element sets with identical and/or similar properties, thus departing from the one property card for every element approach.

VI. References

[1] Droney, C. K., Sclafani, A. J., Harrison, N. A., Grasch, A. D., and Beyar, M. D., "Subsonic Ultra Green Aircraft Research: Phase III – Mach 0.75 Transonic Truss-Braced Wing Design," NASA/CR–20205005698, September 2020.

[2] NASA ISAAC Fact Sheet, FS-2016-12-273-LaRC, 2021

[3] Hyer, Michael W., and Lee, H. H., "The Use of Curvilinear Fiber Format to Improve Buckling Resistance of Composite Plates with Central Holes," *Composite Structures*, Vol. 18, 1991, pp. 239-261.

[4] Nagendra, S., Kodiyalam, A., Davis, J. E., and Parthasarathy, V. N., "Optimization of Tow Fiber Paths for Composite Design," Proceedings of the 36th AIAA/ASME/ASCE/AHS/ASC Structures, Structural Dynamics and Materials (SDM) Conference, AIAA-1995-1275, New Orleans, LA, April 1995.

[5] Waldhart, C. J., Gürdal, Zafer, and Ribbens, C., "Analysis of Tow Placed, Parallel Fiber, Variable Stiffness Laminates," Proceedings of the 37th AIAA/ASME/ASCE/AHS/ASC Structures, Structural Dynamics and Materials (SDM) Conference, AIAA-1996-1569, Salt Lake City, UT, April 1996.

[6] Tatting, Brian F., and Gürdal, Zafer, "Design and Manufacturing of Elastically Tailored Tow Placed Plates," NASA/CR 2002-211919, August 2002.

[7] Tatting, Brian F., and Gürdal, Zafer, "Automated Finite Element Analysis of Elastically-Tailored Plates," NASA CR-2003-212679, December 2003.

[8] Liu, Xin, Liu, Bangde, Kothari, Twinkle, Tian, Su, Long, Leone, Frank, and Yu, Wenbin, "An Integrated Design Tool for Tow-Steered Laminates of Composites in Abaqus and MSC.Patran/Nastran," AIAA SciTech 2023 Forum, AIAA-2023-2594, National Harbor, MD, January 23-27, 2023.

[9] *PATRAN Software Package*, Ver. 2016, MSC Software, Santa Ana, CA, 2016.

[10] *Abaqus Software Package*, Ver. 6.14, Dassault Systèmes Simulia Corp., Pawtucket, RI, 2012.

[11] Zahn, A., and Lovejoy, A. E., "Test and Analysis Correlation of Standard and Hybrid Standard/Thin-ply Composite Notched Test Specimens," AIAA SciTech 2020 Forum, AIAA Paper 2020-0478, Orlando, FL, January 6 – 10, 2020.